Mon. Not. R. astr. Soc. (1991) **251**, 318–329

On the evolution of supernova remnants – II. Two-dimensional calculations of explosions inside pre-existing wind-driven bubbles

G. Tenorio-Tagle,[1] M. Różyczka,[2] J. Franco[3] and P. Bodenheimer[4]

[1] *Instituto de Astrofísica de Canarias, 38200 La Laguna, Tenerife, Spain* and *Max-Planck-Institut für Physik und Astrophysik, Institut für Astrophysik, D–8046 Garching bei München, Germany*

[2] *University of Warsaw Observatory, Al. Ujazdowskie 4, PL–00478 Warszawa, Poland*

[3] *Instituto de Astronomía UNAM, Apartado Postal 70–264, 04510 México DF, México*

[4] *Lick Observatory, Board of Studies in Astronomy and Astrophysics, University of California, Santa Cruz, CA 95064, USA*

Accepted March 12. Received 1991 March 11; in original form 1990 November 15

SUMMARY

Supernova explosions within wind-driven bubbles are studied with 2D hydrodynamical calculations. Two different density distributions for the ejecta are considered: (i) a smooth, unfragmented power-law stratification, and (ii) a fragmented distribution. As in 1D models, the presence of the shell of interstellar swept-up matter causes the rapid evolution of the remnant to the radiative phase. The main 2D effects, for both fragmented and unfragmented ejecta, include: (i) substantial chaotic deviations from a purely radial flow in the remnant interior, (ii) efficient turbulent mixing between the ejecta and the shocked wind, resulting in homogenization of the former wind cavity, and (iii) severe distortion of the wind-driven shell by cooling and Rayleigh–Taylor instabilities. In the case of the fragmented ejecta, additional important effects occur. These, which shape the resulting remnant, include: partial disruption of the shell by fragment impact, the generation of an outer rim of enhanced X-ray emission, and efficient mixing between interstellar, wind, and supernova matter. Explosions in wind cavities display a rich variety of features which may be useful in explaining why many Galactic supernova remnants appear to be in the Sedov phase rather than in the longer lasting radiative phases.

1 INTRODUCTION

For some years, evidence has grown showing the large-scale structures created by stellar energy depositions prior to the supernova (SN) explosion (e.g. Chu, Treffers & Kwitter 1983; Lozinskaya 1988; Dufour 1989; Dubner, Niemela & Purton 1990; Cappa de Nicolau & Olano 1990; Niemela & Cappa de Nicolau 1991; see review by Franco *et al.* 1991b). Similar structures in the LMC have also been investigated by Rosado (1989). The existence of cavities whose formation preceded supernova explosions is strongly advocated on the basis of X-ray, IR, and radio observations of selected SNRs and pulsars (e.g. Braun & Strom 1987; Braun, Goss & Lyne 1989). Moreover, the Crab seems to be embedded within a large bubble, ~90 pc in size (Romani *et al.* 1990), whereas SN 1987A seems to be surrounded by a circumstellar structure with a size of about 1 pc (e.g. Wampler *et al.* 1990). It thus seems very likely that the remnants (SNRs) generated by exploding massive stars evolve in an environment which has been remodelled by winds, outflows, and ionizing quanta from the progenitor. Such a structured environment is a key parameter in defining the structure, shape, and evolution of the resulting remnants.

An additional problem, which can also modify the remnant evolution, is the role played by the early fragmentation of the SN ejecta. This possibility is almost completely unexplored (see Hamilton 1985) but deserves a careful analysis. No doubt the best example of fragmented supernova ejecta interacting with the surrounding gas is found in Cas A (e.g. Braun, Gull & Perley 1987 and references therein), but there are also indications of a possible fragmentation in some other objects (e.g. Hamilton 1985; Braun 1988; Winkler *et al.* 1988; Danziger & Bouchet 1989), including SN 1987A (see Arnett, Fryxell & Müller 1989, and Lucy *et al.* 1989). In the present paper, 2D numerical calculations of SN explosions, with both fragmented and unfragmented ejecta, interacting with wind-driven bubbles are presented and compared with both analytical solutions and 1D numerical simulations.

The effects of the processed environment on the evolution of SNRs has been investigated by several authors (see reviews by Chevalier 1988 and Franco *et al.* 1991b). There are analytical treatments for the evolution of blast waves in cavities with power-law density stratifications, including diagnostics of the energy distributions and expected luminosities (e.g. Cox & Franco 1981; Chevalier 1982; Cox &

Edgar 1983; Nadyozhin 1985). In particular, Chevalier & Liang (1989) recently obtained analytical solutions for the main evolutionary features of the interaction of the SN ejecta with the density structure created by a blue supergiant wind. There is also a growing number of one-dimensional numerical simulations addressing a variety of different expected conditions (e.g. Fabian, Brinkman & Stewart 1983; Dickel & Jones 1985; Shull *et al.* 1985; Band & Liang 1988; Ciotti & D'Ercole 1988). The main results of these works are that the ejecta move in approximately free expansion until they encounter the external wind-driven shell (WDS), and that the remnant cannot be detected inside the bubble. It becomes observable only after the SN blast wave has reached the WDS, and the interaction causes an enhanced soft X-ray as well as optical emission.

Tenorio-Tagle *et al.* (1990, hereafter Paper I) confirmed some of these results and found that the mass contained in the cold WDS is a key parameter defining the evolutionary path. For a WDS mass larger than about 40 times the mass of the ejecta, the Sedov phase is inhibited and the remnants enter the pressure-modified snow-plough phase at early evolutionary time-scales. Less massive WDS are overrun by the blast wave, resulting in a complex multi-shell structure. In all cases, however, the SN ejecta lagged far behind the interstellar swept-up gas, and the model remnants presented a chemical stratification. These calculations, performed under the assumption of spherical symmetry and without considering the possible presence of high-density condensations in the ejecta, already indicated that the details of remnant evolution can be significantly altered by the density structure generated by the previous activity of the progenitor star.

A logical, and certainly needed, step forward is to examine the 2D effects that may appear in the problem and to include the presence of high-density fragments in the SN ejecta. Here we address these important issues and present 2D hydrodynamical models of SNRs evolving in pre-existing wind cavities. Section 2 presents our calculations (methods, assumptions, initial diagnostics and results) for unfragmented explosions, and Section 3 discusses the results of a preliminary study with fragmentation. A brief discussion of the model results is given in Section 4.

2 THE NUMERICAL CALCULATIONS WITH UNFRAGMENTED EJECTA

2.1 Numerical method and physical assumptions

The calculations were performed with the two-dimensional axisymmetric hydrodynamical code described by Różyczka (1985), which includes second-order advection with monotonicity constraint. The computational procedure required the starting model to be prepared for each case independently. This was done with 1D hydrodynamical calculations performed with the Lagrangian code described in Paper I. The 1D model was subsequently transformed on to the 2D Eulerian grid by means of linear interpolation. The 2D grid consisted of 200×200 to 400×400 equally spaced points in cylindrical coordinates (r,z) centred on the explosion site. Symmetry with respect to the mid-plane of the remnant was also assumed, so that only one hemisphere needed to be modelled, which is displayed in the plots as the first quadrant in the (r,z) plane.

The 1D simulation of the wind bubble evolution and the starting models for the supernova explosion proceeded in exactly the same way as described in Paper I. In particular, the density and velocity profiles of the SN ejecta matched those given by Woosley, Pinto & Ensman (1988), and were homologously expanded to 1 pc at the beginning of the run. The resulting density and velocity distributions were $\rho_{ej}\sim r^{-3}$ and $v_{ej}\sim r$, respectively. The effects of the ionizing quanta emitted by the progenitor during its main sequence and later evolutionary phases were neglected. Optically thin radiative cooling in the shocked gas was computed with the cooling function of Raymond, Cox & Smith (1976) for both the 1D and 2D simulations. In all models the density of the unperturbed ambient medium, n_0, was set equal to 1 cm^{-3}. The 2D calculations started at the moment when the blast wave, driven by expanding ejecta, was about to reach the wind-driven shell. Given the small amount of matter in the interior of the wind bubble, only the outermost parts of the ejecta had been processed by the reverse shock. Most of the ejected matter expanded freely within the wind bubble, and thus the kinetic energy before the interaction with the WDS was practically equal to the total energy of the explosion. The models were followed until the outermost shock wave reached the boundary of the computational grid (i.e. for up to $\sim10^5$ yr), and the global remnant properties (total kinetic and thermal energies as well as the integrated total, X-ray, and Hα luminosities) were continuously monitored.

Several cases were calculated assuming different durations of the wind phase, or equivalently, for different masses and locations of the WDS. The results agree globally with the 1D counterparts shown in Paper I. The case of a massive WDS originally located 16 pc away from the explosion site is here analysed in greater detail, and is referred to as Case A. The results of a second model with a smaller WDS, referred to as Case B, is also presented. A typical representation of the 2D starting model is shown in Fig. 1. The blast wave, the reverse shock, and the WDS for Case A are clearly indicated.

2.2 Initial diagnostics

The distributions of mass, momentum, and kinetic energy in the ejecta were set by means of

$$\frac{dM_{ej}}{dr}=4\pi\rho_{ej}(r)r^2=4\pi Ar^{-1}, \tag{1}$$

$$\frac{dP}{dM_{ej}}=v_{ej}(r)=v_{max}\left(\frac{r}{r_{max}}\right), \tag{2}$$

$$\frac{dE_0}{dM_{ej}}=v_{ej}(r)^2, \tag{3}$$

where $A=1.6\times10^{32}$ g, $v_{max}=1.4\times10^4$ km s^{-1}, $r_{max}=r_0+v_{max}t$, and $r_0=1$ pc is the initial ejecta radius for the run. The total mass and energy of the ejecta were set to $M_{ej}=2.5M_\odot$ and $E_0=10^{51}$ erg, and the resulting mass-weighted average and root-mean-squared velocities were $\langle v_{ej}\rangle\simeq5.5\times10^3$ km s^{-1} and $\langle v_{ej}^2\rangle^{1/2}\simeq6.3\times10^3$ km s^{-1} (i.e. roughly half of the maximum velocity).

The interaction between the ejecta and the interior structure of the wind-driven bubble follow the main features described analytically by Chevalier & Liang (1989). Most of

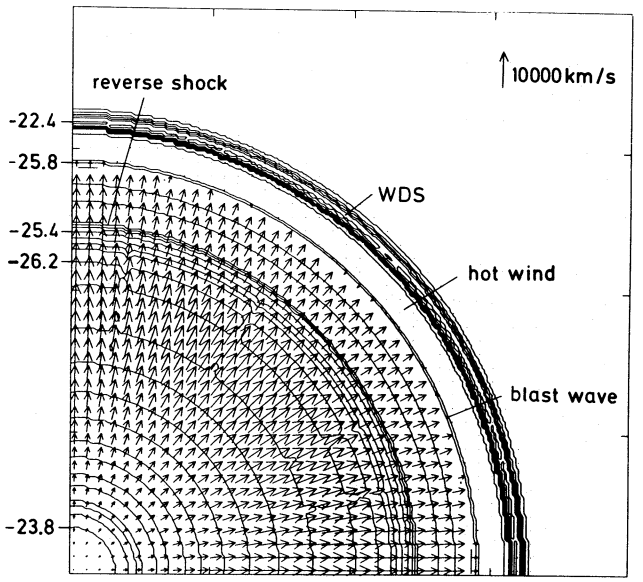

Figure 1. The starting model for Case A (interpolated 1D results, 1500 yr after the explosion). The distance between tick marks on the axis is 5 pc. Logarithmically-spaced constant-density contours are plotted in the (r,z) plane with $\Delta \log \rho = 0.2$, and some of the local values are indicated. The velocity field is represented with arrows whose length is proportional to speed and should be compared with the standard vector given in the right-hand corner.

their formulae, however, cannot be applied to the case $\rho_{ej} \sim r^{-3}$. Nonetheless, some properties can be easily derived. In particular, given that the velocity field is proportional to r, the density profile is not time-dependent and maintains its form $\rho_{ej} = Ar^{-3}$ during the free expansion. This simplifies the treatment of the interaction between the ejecta and the shocked-wind region, which in Case A is initially located between 5 and 15 pc from the source (see Fig. 1). This region has a fairly constant density between $\rho_b \simeq 1$ and 2×10^{-26} g cm^{-3}, and the ejecta reach it with a density of about 4×10^{-26} g cm^{-3}. Thus the reverse shock and the blast wave transmitted into the wind evolve during this phase into nearly constant and comparable densities. The only time-dependent quantity is the velocity of the ejecta, but given that this phase is very short-lived, even this value can be regarded as nearly constant. Taking $\langle v_{ej}^2 \rangle^{1/2}$ as representative of the velocity of the ejecta, the velocity of the shocked wind gas after being overtaken by the transmitted wave can be roughly approximated (in the planar shock approximation) by

$$v_{sw} \sim \frac{(\rho_{ej}/\rho_b)^{1/2}}{(\rho_{ej}/\rho_b)^{1/2}+1} \langle v_{ej}^2 \rangle^{1/2} \sim \frac{2}{3} \langle v_{ej}^2 \rangle^{1/2} \simeq 4 \times 10^3 \text{ km s}^{-1}, \quad (4)$$

the velocity of the transmitted shock is about $4v_{sw}/3$, and the ejecta are shocked with a speed close to

$$\langle v_{ej}^2 \rangle^{1/2} - v_{sw} \simeq 2 \times 10^3 \text{ km s}^{-1}. \quad (5)$$

Thus the reverse shock velocity is well below the value of the ejecta velocity and most of the explosion energy, during the interaction with the shocked wind region, remains as kinetic energy. This phase ends up at a time t_1, when the blast wave strikes the cold and massive WDS

$$t_1 \sim \frac{3\Delta R_{sw}}{4v_{sw}} \simeq 1950 \text{ yr}, \quad (6)$$

where ΔR_{sw} is the initial size of the shocked-wind region.

After t_1, given the large densities in the WDS ($\rho_{WDS} \sim 3 \times 10^{-23}$ g cm^{-3}), the blast wave is abruptly decelerated. This deceleration generates a reflected and a transmitted shock. The reflected shock reduces the velocity of the previously shocked gas and soon catches up with the original reverse shock (this strengthens the reverse shock and causes the full thermalization of the ejecta). The fraction of the ejecta processed by the reflected shock increases as a function of time as

$$f_M \simeq \frac{4\pi A}{M_{ej}} \ln\left(\frac{r_0 + v_{max}t}{R_r}\right) \simeq 0.4 \ln\left(\frac{r_0 + v_{max}t}{R_r}\right), \quad (7)$$

where R_r is the location of the reverse shock. Expansion effects are important and the average density within the shocked region is only a factor of about 2 larger than the initial value of ρ_b. Thus, the approximate location of the reverse shock is

$$R_r \sim \left(\frac{1}{2}\right)^{1/3} R_{WDS} \simeq 12 \text{ pc}. \quad (8)$$

The fraction of the total SN energy entering the shocked region increases as

$$f_E \simeq \left[1 - \frac{R_r^2}{(r_0 + v_{max}t)^2}\right]. \quad (9)$$

The distribution of f_E into thermal and kinetic energies is time-dependent, but ends up as almost purely thermal energy and is deposited near the inner boundary of the WDS. Thus, most of the initial kinetic energy is transformed into heat, causing a pressure increase soon after the blast wave WDS interaction. For simplicity then, at early times one can approximate the fraction in thermal energy as

$$f_{th} \simeq \left[1 - \frac{R_{WDS}^2}{(r_0 + v_{max}t)^2}\right], \quad (10)$$

and the internal pressure is approximated by

$$p_i \simeq \frac{E_0 f_{th}}{\Delta V}, \quad (11)$$

where ΔV is the volume of the shocked region. Provided the shock transmitted into the shell is radiative, then both shock and gas velocities in the shell are comparable and equal to

$$v_s \sim \left(\frac{p_i}{\rho_{WDS}}\right)^{1/2} \simeq \left[\frac{3E_0[1 - R_{WDS}^2(r_0 + v_{max}t)^{-2}]}{4\pi R_{WDS}^3[1 - (R_r/R_{WDS})^3]\rho_{WDS}}\right]^{1/2}$$

$$\simeq 120 \text{ km s}^{-1}. \quad (12)$$

Once the reflected shock has further compressed the shocked region, but before radiative cooling becomes

important, f_{th} tends to $2f_E/3$. This readjustment towards equilibrium, however, lasts only a short period of time because the shock running through the WDS is radiative, and energy losses become important before the whole WDS is completely overrun by the transmitted shock. The WDS receives its $E_0/3$ share of kinetic energy during the interaction. Afterwards, the shell evolves into a momentum-conserving stage.

2.3 Results of calculations

The evolution of the remnant caused by an explosion inside a WDS with a radius of 16 pc is shown in Fig. 2. This run, as stated before, is referred to as Case A in the figures. The calculations agree well with the initial diagnostics of the blast propagating through the wind gas described in the previous subsection. After sweeping through the wind gas, the transmitted blast wave collides with the WDS and sends a transmitted shock into it, while the reflected shock sweeps back towards the explosion site through the wind (which has already been shocked twice: by the wind inner shock and by the SN blast wave), and through the ejecta. The first frames of Fig. 2 show the reverse shock propagating towards the explosion site while thermalizing the ejecta. This shock strengthens as it converges towards the centre of the remnant, leaving behind it a velocity gradient resulting from both convergency effects and non-uniformity of the ejecta. Due to the enforced symmetry of the flow, repeated reflections within the WDS were possible in 1D models, and multiple shock waves with a variety of strengths were observed (see Paper 1). In 2D however, mixing between the wind and ejecta moving at different velocities inhibits the repeated reflections and the flow departs rapidly from a purely radial one. In particular, strong mixing can be observed at a major velocity discontinuity connected with the contact surface between the ejecta and the wind. Wind and ejected matter penetrate each other already in the second frame of Fig. 2, and at later times the contact surface is no longer recognizable.

Meanwhile the transmitted shock sweeps through the WDS. Its propagation velocity is ~ 150 km s^{-1}, and it crosses the shell in $\sim 4 \times 10^3$ yr. The post-shock temperature ($\sim 5 \times 10^5$ K) is close to the maximum of the cooling curve, and the overtaken gas cools on a time-scale shorter than the dynamical one. As a result, the WDS pressure drops below the interior pressure before the whole shell is accelerated. The contact surface between the wind and the swept-up ambient gas (i.e. the inner WDS surface) becomes Rayleigh–Taylor (RT) unstable, leading to the development of RT tongues visible in the last frame of Fig. 2, and to the

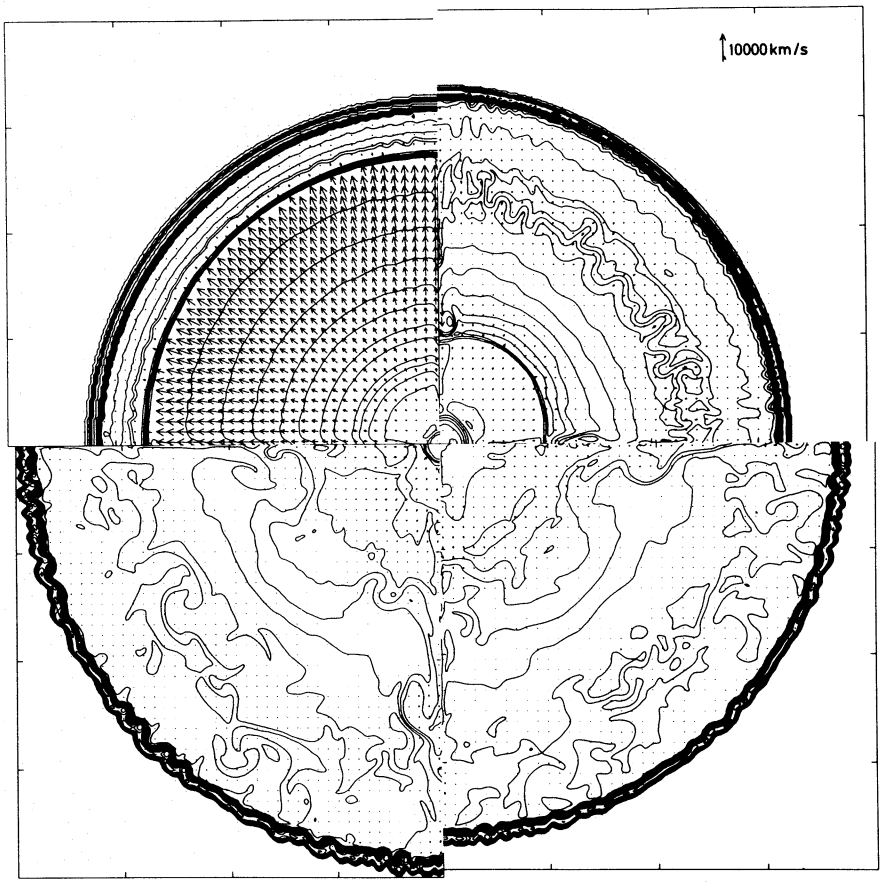

Figure 2. The evolution of Case A. Clockwise from upper left, density distributions in the remnant are shown at $t = 1750$, 4555, 18 000 and 27 360 yr after the explosion. The plots are logarithmic; the contour spacing and the distance between tick marks are the same as in Fig. 1. The individual frames have been successively rotated by 90° so that the r axis is the horizontal axis in the upper right and lower left panels but is the vertical axis in the lower right and upper left.

excitement of the general thin shell instability discussed by Różyczka (1985). It should be stressed here that these instabilities are not (and cannot) be properly resolved in 2D, and that their representation in our models is only qualitatively correct.

The role played by the WDS can be fully appreciated by looking at the run of energy versus time (Fig. 3a). Here, the first 10 000 yr of evolution have been blown up to show the differences from the standard case. Thermalization is delayed until the blast wave meets the WDS, but then within a few hundred years is completed. The flow also clearly avoids the Sedov track, and strong radiative cooling begins to deplete the energy content some 5000 yr after blast. The value of the thermal energy at the end of the run (after 10^5 yr) appears in the standard case only after 10^6 yr of evolution. This implies a tenfold increase in the cooling rate, in the presence of a massive WDS. Total, X-ray and Hα luminosities of the 2D model are plotted against time in Fig. 3b. The figure also shows corresponding luminosities obtained for the standard case. The total luminosity in the standard case peaks after $\sim 3.5 \times 10^4$ yr. On the other hand, the remnant evolving in the processed medium brightens as soon as the blast wave reaches the WDS, i.e. ~ 2700 yr after blast, and then the X-rays and Hα luminosities continuously decrease to lower values, at all times, than those predicted by the standard case.

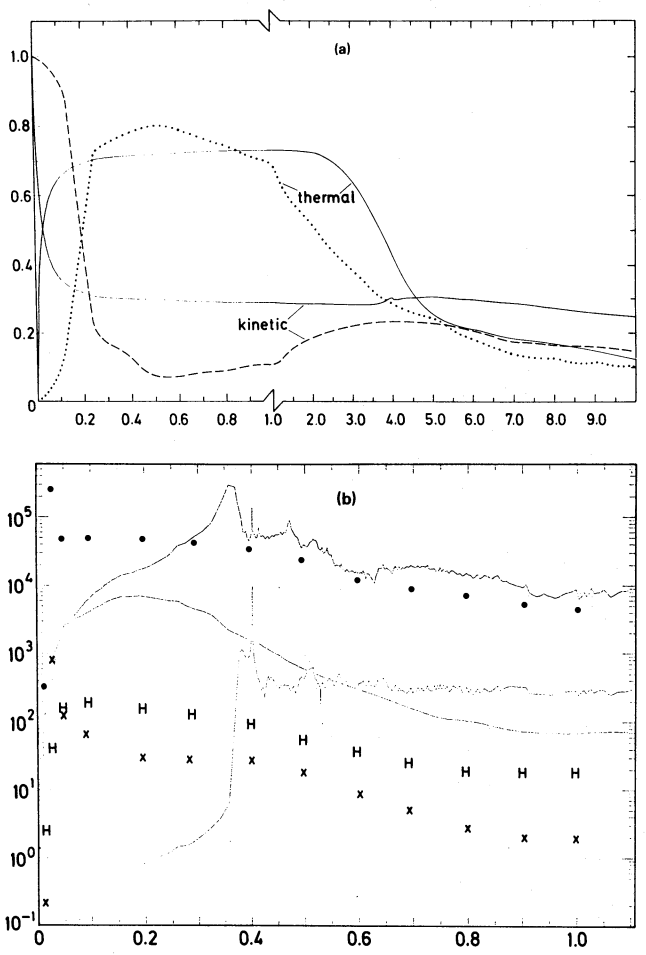

Figure 3. (a) Comparison of the thermal and kinetic energy content of the remnant from case A (broken lines), with the standard case (full lines), as a function of time. (b) Total, X-ray and Hα luminosities of Case A as functions of time compared to those of the standard case (symbols and full lines, respectively).

Fig. 4 shows the results of a second calculation that assumed a WDS 10 pc in radius at the time of the SN explosion (Case B). These conditions are similar to those assumed for the intermediate case in Paper I and the results are qualitatively very similar. The main difference with respect to Case A is caused by the speed of the shock transmitted into the WDS, which in this case exceeds 300 km s^{-1} causing post-shock temperatures $\sim 2 \times 10^6$ K, far larger than the value which leads to maximum cooling. Contrary to Case A, here the transmitted shock does not lose its driving pressure, and it overtakes the shell to propagate into the undisturbed ambient medium (see Fig. 4). At the same time the WDS broadens significantly, and its inner surface becomes ragged due to chaotic motions in the interior of the bubble. Efficient mixing takes place in the remnant interior within a hydrodynamical time, but only between the ejecta and the previously injected wind gas. In none of the calculated models is there a clear sign of mixing of ejected and swept-up interstellar matter, which remains separated in the external parts of the shell.

3 FRAGMENTED EJECTA

The first suggestion that the ejecta could be fragmented by Rayleigh–Taylor instabilities was given by Falk & Arnett (1973). Chevalier (1976) discussed the development of these instabilities when the density distribution of the ejecta is approximated by a power law, and the resulting growth was computed by Chevalier & Klein (1978) with 'low-resolution' 2D simulations. More refined and detailed studies of the process, using 2D and 3D codes with more realistic models for the ejecta, have been recently performed by Arnett *et al.* (1989) and Müller, Fryxell & Arnett (1990). These studies, which have impressive temporal and spatial resolution, show that the RT instabilities develop almost immediately after the explosion and that the resulting fragments have density enhancements in the range 3–10 with respect to the rest of the ejected matter (the 'inter-fragment' medium). In addition, Kelvin–Helmholtz instabilities are present, giving a 'mushroom' appearance to the recently formed fragments. Once fragmentation occurs, and in the absence of any further disturbance, the fragments simply expand together with the rest of the flow.

3.1 Initial model and physical assumptions

To calculate the effects caused by fragmented ejecta in the evolution of a supernova remnant, one has to follow the fragment evolution from their formation site (at locations $\leq 10^{11}$ cm from the explosion centre) until they are thermalized, at distances which are several orders of magnitude larger, $\sim 10^{19}$–10^{20} cm. There is no numerical scheme available that can calculate, with the required resolution, the details of the evolution over the range of physical dimensions imposed by the problem. Furthermore, the situation actually requires a full 3D calculation, so that the axisymmetric calculation presented here is not guaranteed to reveal all the instabilities that are present. Because the resultant fast-moving fragments or knots (FMKs) expand together with the interfragment

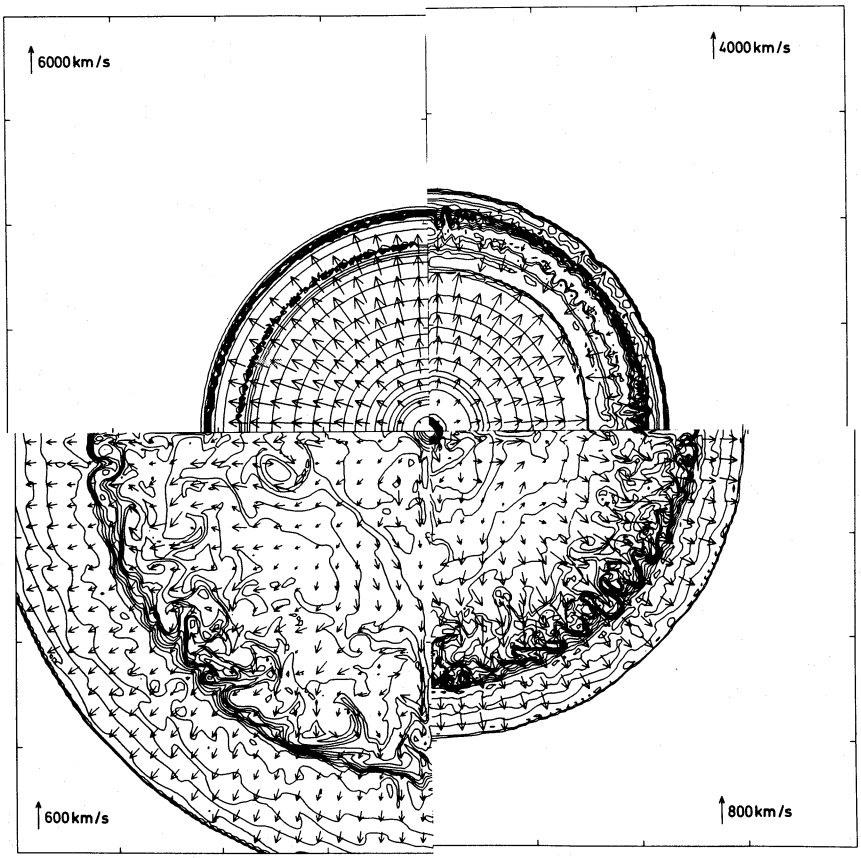

Figure 4. The evolution of Case B. Clockwise from upper left, density distributions in the remnant are shown at $t = 1250$, 1903, 5500 and 19 050 yr after the explosion. The plots are logarithmic; the contour spacing and the distance between tick marks are the same as in Fig. 1.

medium, we assume that they simply undergo a homologous growth, maintaining their density contrast, until they reach the reverse shock. From the previous calculations, we know that the ejecta travel almost unimpeded until the blast wave interacts with the outer shell containing the interstellar swept-up matter. The reverse shock strengthens after impact and thermalizes the kinetic energy released during the explosion. It will be only then that the FMKs would modify their trajectory and homologous growth defined during fragmentation. Here the calculations are extended in a preliminary study of the role played by the fragments.

The starting model was prepared, following the same procedure described in the previous section, for each case independently. The 2D calculations started at the moment when the blast wave driven by the expanding ejecta was about to reach the WDS. Due to the low densities of the wind bubble interior, as discussed before, only the outermost parts of the ejecta had been thermalized at that time, and thus the kinetic energy of the ejecta was still practically equal to the total explosion energy (E_0). The main features of the calculated flow were again tested with the analytical approximations described in Section 2.

The unshocked ejecta were then rearranged into a collection of identical fragments by arbitrarily defining their number, location, angular size, length, and relative density enhancement with respect to the local ambient value. The only restriction enforced in this procedure was the strict conservation of mass and kinetic energy during the rearrangement process. Thus a corresponding amount of matter was removed from the interfragment region, and the original velocity field was preserved everywhere on the grid. Such a procedure also preserves the homologous growth of the flow. Additionally, it was assumed that the collection of smaller and less massive fragments generated by the RT instability are not dynamically, nor energetically, as important as the large fast-moving knots selected for the runs. Magnetic fields and the effects caused by photoionization from the progenitor star (either during its main sequence or Wolf-Rayet phases) were neglected. Again, optically thin radiative cooling of shocked gas, using the cooling function of Raymond *et al.* (1976), was allowed for in both the 1D and 2D calculations. The density of the unperturbed ambient medium (n_0) was set, in all models, equal to 1 cm^{-3}. The models were followed for up to $\sim 10^5$ yr after explosion, and their global properties (including total kinetic and thermal energy, and total X-ray and Hα luminosities) were continuously monitored.

3.2 Results of calculations

A typical representation of the 2D starting model with fragments is shown in the first frame of Fig. 5. To have a direct comparison with Case A described before, the WDS is located at a distance of 16 pc away from the explosion site.

Most of the former wind matter has already been overrun and accelerated to high speeds by the blast wave. The location of the reverse shock, which has partially decelerated the outermost parts of the ejecta (i.e. the least dense but fastest moving parcels of the ejecta), is clearly apparent in the figure. The four identical fragments selected for this run were placed interior to the reverse shock. The angles subtended by the four fragments in the figure add to about 20°, and each fragment has a radial extent of about 30 per cent of the present radius of the unshocked ejecta. The maximum density of the knots is a factor of 10 larger than the present mean value in the local inter-fragment medium. At this time, 1700 yr after the explosion, the total amount of kinetic energy remains close to the initial value, 10^{51} erg.

The set of frames displayed in Fig. 5 illustrates a series of transient events resulting from the ejecta-WDB interaction. In the first frame the blast wave sweeps through the hot wind region and is about to strike the WDS. The outer parts of the ejected matter have been partially decelerated by a weak reverse shock, and, interior to this, four fragments selected for the run expand homologously away from the explosion site. Upon the interaction of the blast wave with the WDS, as discussed before, a transmitted shock begins to accelerate the innermost zones of the WDS while a second and stronger reverse shock thermalizes the incoming matter. This reverse shock decelerates the incoming material almost to rest (and sometimes even to inward-directed velocities). The second frame of Fig. 5 (at a time $t_{sn} = 2160$ yr after the explosion) shows the location of the new reverse shock, close to the inner boundary of the WDS, where the low-density parts of the shocked ejecta have acquired a low negative (inward) velocity. The first and weaker reverse shock is now located deeper in the flow and is strongly deformed on the borders of the FMKs, given that it cannot penetrate and move through the denser fragments as quickly as it can move into the inter-fragment medium. Some 500 yr later (third frame), the FMKs collide with the WDS to become thermalized, and they transmit, at the location of impact, new and even stronger shocks into the WDS. In what follows these stronger, and localized, shocks will be simply referred to as the 'stronger shocks'. At $t_{sn} = 3100$ yr after the explosion, all reverse shocks merge and their joint action leads to an inward flow in the remnant interior, which rapidly thermalizes the rest of the ejecta.

The energy and momentum rates injected by the interacting fragments, which heat and accelerate the WDS at the particular places of impact, are larger than those injected by the inter-fragment medium by a factor ρ_{fmk}/ρ_{ifm} (where ρ_{fmk} and ρ_{ifm} are the densities of the FMKs and inter-fragment medium at the time of impact, respectively). The velocity of the stronger shocks, V_{ss}, is correspondingly larger than the weaker transmitted shock velocity generated by the inter-

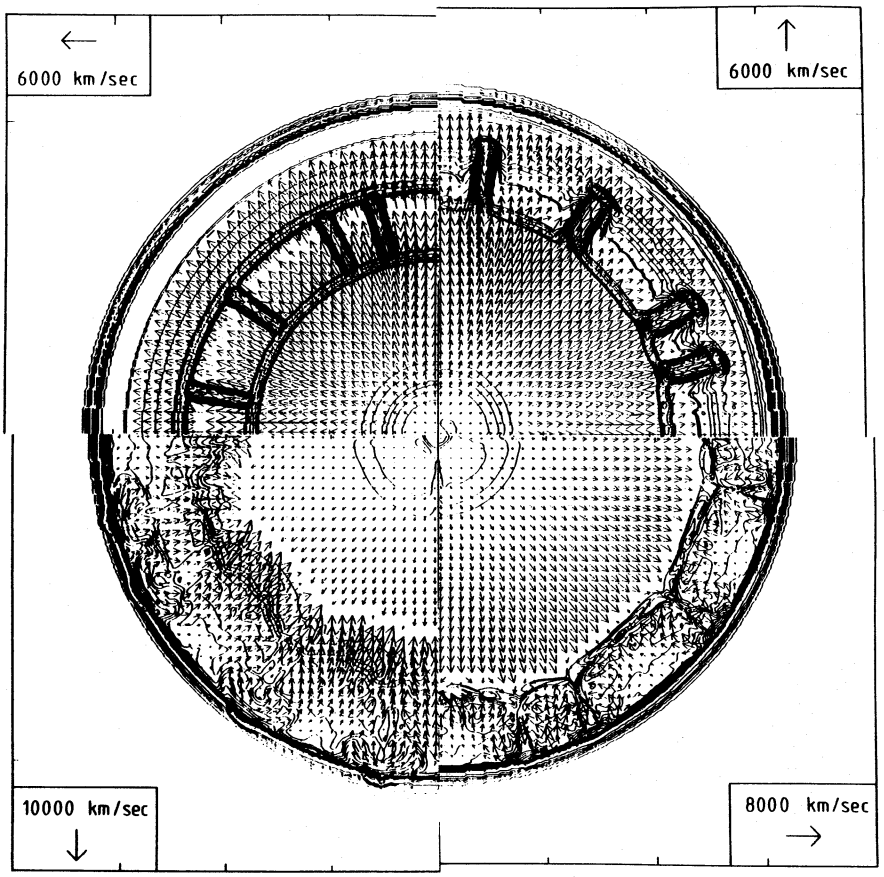

Figure 5. Evolution of fragmented ejecta. Clockwise from upper left, density distributions in the remnant are shown at times of 1700, 2160, 2760 and 3100 yr after the explosion. The plots are logarithmic; the contour spacing is $\Delta \log \rho = 0.2$, and the distance between tick marks is 5 pc. The velocity field is represented by arrows, the length of which should be compared with the standard vector shown in every plot.

fragment medium, V_{ws}. A rough estimate of these velocities, assuming planar shocks and neglecting time-dependent effects, can be obtained by the analytical approximations for two colliding streams. Within this simple scheme, the velocities of all transmitted shocks can be related by

$$V_{ss} \sim \left(\frac{\rho_{fmk}}{\rho_{ifm}}\right)^{1/2} V_{ws}.$$

This approximate scaling is in fair agreement with the shock velocity differences generated at different locations of the WDS: $V_{ss} \sim 3V_{ws} \sim 500$ km s^{-1}. The impact of the FMKs against the WDS raises the temperature to several times 10^6 K at the locations of impact, inhibiting strong radiative cooling. As a result, the stronger shocks are able to traverse the WDS and propagate into the unperturbed gas ahead of it. These events lead to a pressure field in the shocked region which is position-dependent, containing large-pressure sites. From these, lateral pressure gradients result in non-radial motions, and the flow becomes chaotic in a short time-scale.

The effects caused by the FMKs on the WDS are shown in Fig. 6. The stronger transmitted shocks, now moving into the unperturbed gas, behave as a set of new explosion centres and rapidly acquire hemispherical shapes. The WDS now appears punctured or fragmented, and the resulting chaotic velocity field enhances the mixing between ejecta, wind, and the disrupted gas from the WDS. Neighbouring impacts favour merging of the transmitted disturbances which end up as a single leading shock surface that wraps around the remaining sections of the WDS. This shock has a large speed (>400 km s^{-1}) and creates an outer rim of X-ray emitting gas around the slower sections of the WDS, which are heated by weaker transmitted shocks and which radiate strongly in the optical frequency range. Naturally, these sections of the remnant may appear to an observer as large-scale Hα filaments or sheets.

The final stages of the calculated evolution are shown in Fig. 7. Strong radiative cooling behind the outermost shock produces, as in the late stages of any shock evolution, the condensation of the swept-up matter into a thin, cool, dense, and rapidly decelerating outer shell. The slow sections of the former WDS became greatly distorted by the chaotic motions inside the remnant, and eventually merge with the outer shell. After 10^5 yr of evolution, they compose a strongly deformed and clumpy dense shell, with dimensions almost twice the size of the original WDS.

In terms of the energy evolution, there are major departures from the standard case (see Fig. 8a), and also from the previous results without fragmentation (compare with Fig. 3a). The runs of thermal and kinetic energies are shown and compared with those derived from the standard case in Fig. 8a. As stated above, thermalization is efficient in the blast wave interaction with the WDS, some 1700 yr after blast. The subsequent thermalization of the FMKs leads to well-localized thermal energy enhancements within the remnant. Each of these, in turn, leads to an almost adiabatic re-expan-

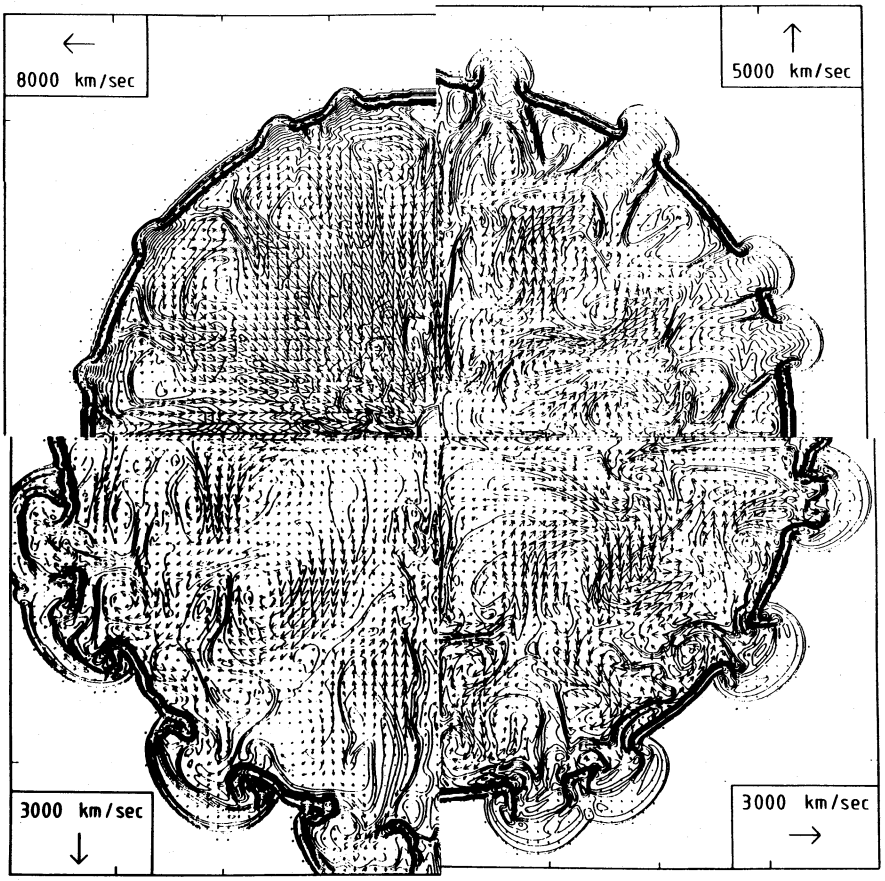

Figure 6. The same as Fig. 5 at times 3900, 6250, 9870 and 15 950 yr after the explosion.

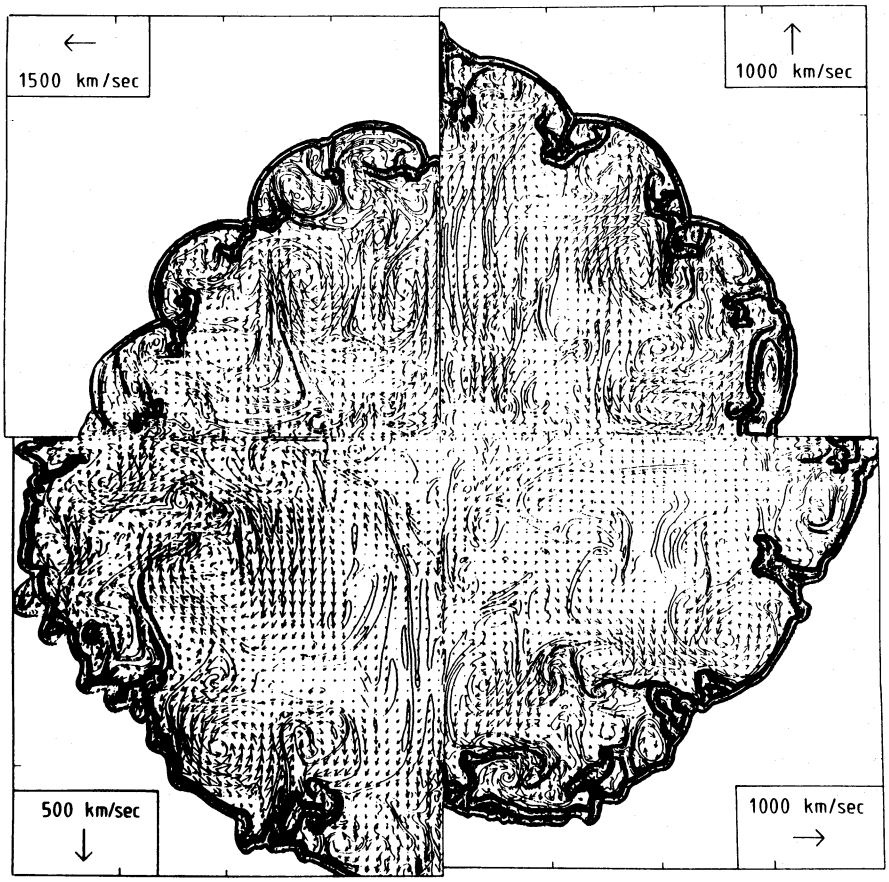

Figure 7. The same as Fig. 5 at times 25 300, 42 000, 63 900 and 90 300 yr after the explosion. The distance between tick marks is 8 pc.

sion, and thus a fraction of the localized thermal energy excess is then almost immediately reconverted into kinetic energy of the hot gas, creating spikes in the corresponding tracks. The maximum thermal energy (E_{th}), immediately after the impact of the FMKs, is about $0.6\,E_0$. Some 500 yr later, after re-expansion of the pockets of hottest gas, E_{th} declines and E_{kin} reaches a peak value of about $0.47\,E_0$. The subsequent evolution, after the stronger shocks have penetrated into the interstellar medium and the excess localized energy has been shared by the whole remnant, becomes smoother with the characteristic appearance of a thermal piston driving the evolution. Note, however, that the process is not adiabatic; rather, there is a strong and clear decline in the energy content starting some 5000 yr after the explosion. Some 10^5 yr later, radiative cooling (see Fig. 8b) has reduced the value of E_{th} to below $0.05\,E_0$, while the total kinetic energy has a value of the order of $0.1\,E_0$.

The preliminary calculations have assumed that a collection of fragments (which we identify with the so-called fast-moving knots, or FMKs, observed in some remnants) expand, preserving their density contrast and velocity field until they interact with the massive WDS. Several of these calculations have been performed assuming different initial conditions (i.e. number, locations, sizes, and masses of FMKs, as well as different initial sizes of wind-driven bubbles) and, even though many details are different, the main evolutionary features are qualitatively the same. The results presented here are thus representative of the various calculated cases.

4 DISCUSSION

Given the strong observational evidence for shells produced by massive stars prior to their explosion as supernovae, it now seems clear that the evolution of the standard (constant-density) case should be regarded as an idealized theory exercise, which provides an appropriate frame of reference to investigate a more realistic evolution. The calculations here described, along with previous analytic and numerical estimates mentioned in the text, indicate several modifications caused by the density stratification left by a powerful stellar wind prior to the explosion. The crucial factor determining the evolutionary path of such remnants and the fate of the pre-existing WDS is the velocity of the shock wave transmitted into the shell. If the latter is fast enough to prevent strong cooling (say if $V \geq 300$ km s^{-1}), the whole shell expands while the wave overtakes it and propagates into the undisturbed ambient medium. Thus low-mass WDS remnants should follow an evolution close to the standard solution, except for a short phase of strong Hα emission immediately after the blast wave interacts with the WDS (see Fig. 6 in Paper I). This short phase may be associated with the optical emission of some historical remnants. On the other hand, if the post-shock temperatures fall in the range of maximum cooling, the pressure in the shell drops, and Rayleigh–Taylor and thin shell instabilities develop.

The presence of a massive WDS then has a profound effect on the evolution and appearance of SN remnants. This case, given the measured mechanical energy in winds of

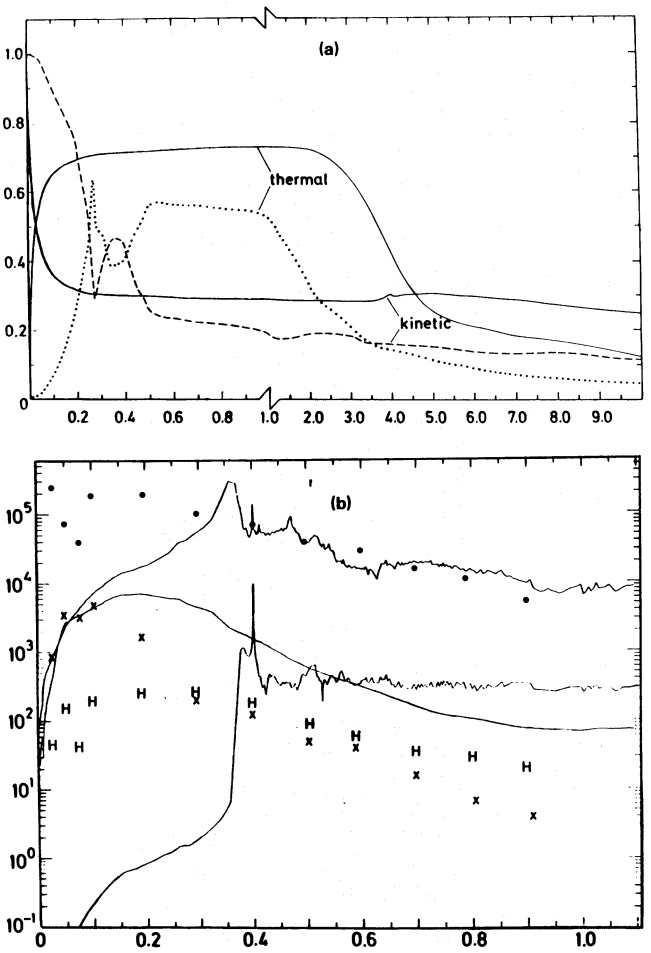

Figure 8. (a) Thermal and kinetic energy content of the remnant shown in Figs 5–7, as a function of time (dotted and dashed lines, respectively), compared with the energetics of the standard case (solid lines). The time is given in units of 10^4 yr, with the first 10^4 yr blown up to show the rapid changes that take place during the early evolution. (b) Total, X-ray and Hα luminosities of the remnant shown in Figs 5–7, as a function of time, compared to those obtained for the standard solution (symbols and full lines, respectively). Time is given in units of 10^5 yr.

massive stars and/or the fact that most supernova explosions are spatially correlated, is perhaps the most common case in nature. In addition, fragmented ejecta produce a rich variety of other new events. The main departures from the standard solution are:

(i) The remnants age rapidly, as all evolutionary phases (with the exception of thermalization) are substantially speeded up. After the explosion, given the small amount of matter in the wind-driven bubble, the almost freely moving ejecta undergo only partial thermalization. However, when the shock strikes the massive shell of interstellar swept-up matter, thermalization is rapidly completed. In the standard case after thermalization, the remnant enters its Sedov evolutionary phase. Here, in the presence of a massive WDS, the evolution resembles that of remnants in a high-density environment (with $n_0 \geq 10^5$ cm^{-3}; see Shull 1980; Wheeler, Masurek & Sivaramakrishnan 1980), where the quasi-adiabatic Sedov phase is totally inhibited. Upon thermalization, the remnant radiates rapidly its thermal energy content and misses the combination $E_{th} = 0.7E_0$, $E_{kin} = 0.3E_0$, that characterizes the Sedov solution. Instead, it directly enters the pressure-modified snow-plough stage.

(ii) Upon thermalization of the ejecta, the total and Hα luminosities of the remnant are greatly enhanced, up to values that in the standard case are expected only after a few times 10^4 yr. Thus, the observable phase occurs at much earlier times. Strong radiative cooling then rapidly dissipates the thermal energy content and 10^5 yr after the explosion the remnant has an Hα luminosity which in the standard case is only expected after 10^6 yr of evolution. In X-rays the luminosity drops even more abruptly. Thus, 10^5 yr after blast, the remnants have radiated most of the explosion energy.

(iii) In all cases the interiors of 2D remnants are fairly homogeneous, due to the complex velocity field generated by the instabilities. Such a velocity field, which can be regarded as turbulent, destroys the initial flow stratifications and results in a complete mixing of all gas elements in the remnant interior. The chemical stratification present in 1D simulations, then, is only due to the restrictive geometry of the flow.

(iv) The role played by the impacts of FMKs is crucial in defining the filamentary structure of SNRs, as shown in Figs 5–7 and as inferred from the observations (Braun *et al.* 1987). FMKs inject a relatively large amount of energy per unit surface to the shell and lead, upon thermalization, to strong transmitted shocks, capable of traversing and disrupting the WDS. They later emerge at high speed into the unperturbed ambient gas. A series of such punctures of the shell soon connects the various transmitted shocks into a single surface, which envelopes the whole remnant with an outer rim of X-ray emitting gas. Eventually this hot gas also cools down and condenses into a secondary thin outer shell, while the remaining sections of the original WDS, deformed by chaotic motions inside the remnant, begin to catch up with it. At this stage, however, the remnant will have already radiated most of the energy deposited by the explosion, making its detection improbable.

(v) The collision of FMKs with the pre-existing massive WDS leads also to rapid mixing of the thermalized ejecta, the previously existing wind, and the disrupted interstellar matter originally locked up in the WDS. This mixing is strongly favoured by the chaotic motions that develop within the remnant interior.

These results have a direct impact in interpretations of the statistical properties of SNRs (e.g. Clark & Caswell 1976; Green 1984; Caswell 1988 and references therein). Early studies, despite many shortcomings, were interpreted in terms of the Sedov solution. Such an interpretation was strengthened by the results of Lozinskaya (1980) who found that most, if not all, old optical SNRs with radii larger than 8 pc in the Galaxy follow the velocity-size relationship expected from the Sedov, or quasi-adiabatic, evolutionary phase. Similar analyses were performed in the Large Magellanic Cloud (Rosado 1986), but the slope in this case was interpreted in terms of an adiabatic evolution modified by evaporative effects (e.g. McKee & Cowie 1975; it can also be explained by adiabatic wind-driven shells or blast waves in decreasing density profiles, see Tenorio-Tagle, Bodenheimer & Franco 1988). Large optical remnants following adiabatic tracks, however, are difficult to reconcile with the standard

evolutionary framework, mainly because this phase should only be detectable at X-ray frequencies, and only a small fraction (about 30 per cent) of the known galactic radio supernovae has been detected in X-rays (e.g. Aschenbach 1988; Seward 1988; Smith 1988). In addition, one may wonder where all the radiative and momentum-conserving remnants are. Statistically speaking, they should exceed the number of adiabatic remnants by large factors.

The observed remnant shells can, on the other hand, be interpreted as the recently energized shells of matter swept by the previous winds. In this scenario, the dimensions of SNRs are largely determined by the size of the original shell, and the observed Hα remnant is the massive WDS, lighted up by the shock transmitted by the SN blast wave. Note that, for standard wind parameters of massive stars, the dimensions of the target shells fall in the range of values expected in the standard solution during the Sedov phase (5–30 pc). The PV-work done by the re-thermalized wind-driven cavity results in a remnant with a kinetic energy content of about $0.3E_0$, similar to the one expected from the Sedov evolution, and most of this energy is stored in the re-accelerated wind-driven shell. Therefore, observed remnants, while strongly radiating, have sizes matching those expected for the Sedov phase. Such a mere coincidence can certainly become a major source of misclassification, and may explain why the optical galactic remnants seem to be in the Sedov phase and not in the longerlasting momentum-conserving stage. A detailed look at the expansion velocities determined for galactic remnants (Lozinskaya 1980) indeed shows several velocity values below 250 km s^{-1}, characteristic of radiative shocks. Such a misclassification when applied to radio remnants is, together with unreliable distance estimates and selection effects (see Green 1984), another important source of error in derivations and interpretations of the so-called 'number–size' (N–D) relationship (see Caswell 1988 and references therein). If the size of remnants is mainly determined by the dimensions of the wind cavities within which explosions have occurred, and not by their growth expected from the standard evolution, then the number of remnants with a size smaller than D (a reference diameter) may not imply the number of explosions during the evolutionary time required to reach the reference diameter, but rather the number of explosions that have recently occurred within WDSs with a dimension smaller than D. Clearly, this also implies that estimates of supernova rates derived from such a relationship should be taken with extreme caution.

The effects of the FMKs, on the other hand, are also expected to shape up the environment of an OB association. The cavities and shells generated by the winds from massive stars and the first SN explosions will be subjected to an almost continuous bombardment by the FMKs produced by the fragmented explosions of spatially correlated type II supernovae. Such events naturally lead to the disruption of the shell of swept-up matter which otherwise would remain continuous (Tenorio-Tagle *et al.* 1986; Tomisaka 1991) in the presence of the extended exponential H I disc (Dickey & Lockman 1990), inhibiting blowouts, fountains, and galactic chimneys. It is thus likely, at least in the case of the Galaxy, that thermalization of the FMKs produced by an OB association is an event that, together with radiation-driven fountains (i.e. Franco *et al.* 1991a), allows for the connection between the disc and the halo.

ACKNOWLEDGMENTS

It is a pleasure to thank Joaquín Bohigas for useful information about optical and radio remnants, and Michael Rosa and Margarita Rosado for informative talks about ring-shaped nebulae. We also acknowledge the comments provided by an anonymous referee. JF and GT-T acknowledge travel grants from CONACyT–México, and JF thanks the hospitality of the Max-Planck Institut für Astrophysik, Garching. MR was supported by the grant G–MEN–156/90 from the Polish Ministry of Education, and part of his work was done while he was a visiting research scientist at Lick Observatory under the auspices of the Center for Star Formation Studies.

REFERENCES

Arnett, D., Fryxell, B. & Müller, E., 1989. *Astrophys. J. Lett.*, **341,** L63.

Aschenbach, B., 1988. In: *Supernova Remnants and the Interstellar Medium, IAU Colloq. No. 101*, p. 227, eds Roger, R. S. & Landecker, T. L., Cambridge University Press, Cambridge.

Band, D. L. & Liang, E. P., 1988. In: *Supernova Remnants and the Interstellar Medium, IAU Colloq. No. 101*, p. 69, eds Roger, R. S. & Landecker, T. L., Cambridge University Press, Cambridge.

Braun, R., 1988. In: *Supernova Remnants and the Interstellar Medium, IAU Colloq. No. 101*, p. 227, eds. Roger, R. S. & Landecker, T. L., Cambridge University Press, Cambridge.

Braun, R. & Strom, R. G., 1987. *Astr. Astrophys.*, **164,** 193.

Braun, R., Goss, W. M. & Lyne, A. G., 1989. *Astrophys. J.*, **340,** 355.

Braun, R., Gull, S. F. & Perley, R., 1987. *Nature*, **327,** 395.

Cappa, de Nicolau, C. & Olano, C. A., 1990. *Rev. Mex. Astr. Astrofiz.*, **21,** 269.

Caswell, J. L., 1988. In: *Supernova Remnants and the Interstellar Medium, IAU Colloq. No. 101*, p. 269, eds Roger, R. S. & Landecker, T. L., Cambridge University Press, Cambridge.

Chevalier, R. A., 1976. *Astrophys. J.*, **207,** 872.

Chevalier, R. A., 1982. *Astrophys. J.*, **258,** 790.

Chevalier, R. A., 1988. In: *Supernova Remnants and the Interstellar Medium, IAU Colloq. No. 101*, p. 31, eds Roger, R. S. & Landecker, T. L., Cambridge University Press, Cambridge.

Chevalier, R. A. & Klein, R. I., 1978. *Astrophys. J.*, **219,** 994.

Chevalier, R. A. & Liang, E. P., 1989. *Astrophys. J.*, **344,** 332.

Chu, Y.-H., Treffers, R. R. & Kwitter, K. B., 1983. *Astrophys. J. Suppl.*, **53,** 937.

Ciotti, L. & D'Ercole, A., 1988. *Astr. Astrophys.*, **215,** 347.

Clark, D. H. & Caswell, J. L., 1976. *Mon. Not. R. Astr. Soc.*, **174,** 267.

Cox, D. P. & Edgar, R., 1983. *Astrophys. J.*, **265,** 443.

Cox, D. P. & Franco, J., 1981. *Astrophys. J.*, **251,** 687.

Danziger, I. J. & Bouchet, P., 1989. In: *Evolutionary Phenomena in Galaxies*, p. 283, eds Pagel, B. & Beckman, J., Cambridge University Press, Cambridge.

Dickel, J. R. & Jones, E. M., 1985. *Astrophys. J.*, **288,** 707.

Dickey, J. M. & Lockman, F. J., 1990. *Ann. Rev. Astr. Astrophys.*, **28,** 215.

Dubner, G. M., Niemela, V. S. & Purton, C., 1990. *Astr. J.*, **99,** 857.

Dufour, R. J., 1989. *Rev. Mex. Astr. Astrofis.*, **18,** 87.

Fabian, A. C., Brinkman, W. & Stewart, G. C., 1983. In: *Supernova Remnants & Their X-ray Emission, IAU Symp. No. 101*, p. 119, eds Danziger, J. & Gorenstein, P., Reidel, Dordrecht.

Falk, S. W. & Arnett, D., 1973. *Astrophys. J. Lett.*, **180,** L65.

Franco, J., Ferrini, F., Ferrara, A. & Barsella, B., 1991a. *Astrophys. J.*, **366,** 443.

Franco, J., Tenorio-Tagle, G., Bodenheimer, P. & Różyczka, M., 1991b. *Publs. Astr. Soc. Pacif.*, in press.

Green, D. A., 1984. *Mon. Not. R. Astr. Soc.*, **209,** 449.
Hamilton, A. J. S., 1985. *Astrophys. J.*, **291,** 523.
Lozinskaya, T. A., 1980. *Astr. Astrophys.*, **84,** 26.
Lozinskaya, T. A., 1988. In: *Supernova Remnants and the Interstellar Medium, IAU Colloq. No. 101*, p. 95, eds Roger, R. S. & Landecker, T. L., Cambridge University Press, Cambridge.
Lucy, L. B., Danziger, I. J., Gouiffes, C. & Bouchet, P., 1989. In: *Structure & Dynamics of the Interstellar Medium, IAU Colloq. No. 120*, p. 164, eds Tenorio-Tagle, G., Moles, M. & Melnick, J., Springer, Berlin.
McKee, C. F. & Cowie, L. L., 1975. *Astrophys. J.*, **195,** 715.
Müller, E., Fryxell, B. & Arnett, D., 1991. In: *Chemical and Dynamical Evolution of Galaxies*, eds Ferrini, F., Franco, J. & Matteucci, F., Giardini, Pisa.
Nadyozhin, D. K., 1985. *Astrophys. Space Sci.*, **112,** 225.
Niemela, V. S. & Cappa de Nicolau, C., 1991. *Astr. J.*, **101,** 572.
Raymond, J. C., Cox, D. P. & Smith, B. W., 1976. *Astrophys. J.*, **204,** 290.
Romani, R. W., Reach, W. T., Koo, B. C. & Heiles, C., 1990. *Astrophys. J. Lett.*, **349,** L51.
Rosado, M., 1986. *Astr. Astrophys.*, **160,** 211.
Rosado, M., 1989. *Rev. Mex. Astr. Astrofiz.*, **18,** 105.
Różyczka, M., 1985. *Astr. Astrophys.*, **143,** 59.
Seward, F. D., 1988. In: *Supernova Remnants & the Interstellar Medium, IAU Colloq. No. 101*, p. 115, eds Roger, R. S. & Landecker, T. L., Cambridge University Press, Cambridge.
Shull, J. M., 1980. *Astrophys. J.*, **237,** 709.
Shull, P. Jr, Dyson, J. E., Kahn, F. D. & West, K. A., 1985. *Mon. Not. R. Astr. Soc.*, **212,** 799.
Smith, A., 1988. In: *Supernova Remnants & the Interstellar Medium, IAU Colloq. No. 101*, p. 119, eds Roger, R. S. & Landecker, T. L., Cambridge University Press, Cambridge.
Tenorio-Tagle, G., Bodenheimer, P. & Franco, J., 1988. In: *High Energy Astrophysics,* p. 77, ed. Börner, G., Springer-Verlag, Berlin.
Tenorio-Tagle, G., Bodenheimer, P. & Różyczka, M., 1986. *Astr. Astrophys.*, **182,** 120.
Tenorio-Tagle, G., Bodenheimer, P., Franco, J. & Różyczka, M., 1990. *Mon. Not. R. astr. Soc.*, **244,** 563 (Paper I).
Tomisaka, K., 1991. In: *IAU Symp. No. 144,* Disc–halo connections, ed. Bloeman, H., Reidel, Dordrecht.
Wampler, E. J., Wang, L., Baade, D., Banse, K., D'Odorico, S., Gouiffes, C. & Tarenghi, M., 1990. *Astrophys. J. Lett.*, **362,** L13.
Wheeler, J. C., Masurek, T. J. & Sivaramakrishnan, A., 1980. *Astrophys. J.*, **237,** 781.
Winkler, P. F., Tuttle, J. H., Kirshner, R. P. & Irwin, M. J., 1988. In: *Supernova Remnants & the Interstellar Medium, IAU Colloq. No. 101*, p. 65, eds Roger, R. S. & Landecker, T. L., Cambridge University Press, Cambridge.
Woosley, S. E., Pinto, P. A. & Ensman, L., 1988. *Astrophys. J.*, **324,** 466.